Surface & Coatings Technology 206 (2012) 2330–2336

Contents lists available at SciVerse ScienceDirect

Surface & Coatings Technology

journal homepage: www.elsevier.com/locate/surfcoat

Development and characterization of electro deposited Nickel–Titanium Carbo Nitride (TiCN) metal matrix nanocomposite deposits

G.N.K. Ramesh Bapu *, Sobha Jayakrishnan

Electroplating and Metal Finishing Technology Division, CSIR-Central Electrochemical Research Institute, Karaikudi-630 006, Tamilnadu, India

ARTICLE INFO

Article history:
Received 13 July 2011
Accepted in revised form 30 September 2011
Available online 23 October 2011

Keywords:
Nanocomposite
Hardness
Wear resistance
Corrosion resistance
SEM
XRD

ABSTRACT

The effects of electrochemical parameters on the development of Nickel–Titanium Carbo Nitride (TiCN) metal matrix nanocomposite deposits were studied in Watts type nickel bath. The extent of TiCN incorporation into nickel matrix was studied with respect to TiCN particle concentration ranged between 2 and 15 g l^{-1}, current density ranging from 2 to 10 Ad m^{-2}, bath pH from 2 to 5 and a bath temperature range of 30–70 °C. Effects of TiCN particle incorporation on surface morphology, crystal structure, micro hardness, wear resistance and corrosion resistance of the composite deposits were studied. It was found that the incorporation of TiCN particles in the composite deposit increased with increasing TiCN content in the bath. Operating the bath with 6 g l^{-1} TiCN particle concentrations at 4 Ad m^{-2}, at 50 °C, and at pH 4 gave about 23.9 vol.% TiCN incorporation in the composite deposit. The results showed that the codeposition of TiCN particles with nickel modified the surface morphology of nickel and its preferred orientation. The Ni–TiCN composite deposits showed better corrosion resistance in 3.5 wt.% NaCl solution and high hardness and wear resistance than nickel electrodeposited under the same conditions.

1. Introduction

Electrodeposition has a number of advantages over other physical deposition techniques since it is a low cost process and can be used for many practical applications. The incorporation of chemically inert ceramic particles into metallic matrix to produce particle dispersed metal matrix composite (PDMC) coatings has attracted much interest for decades [1]. Corrosion and wear resistance of mechanical parts are major concerns and the common way of increasing wear resistance is the codeposition of hard particles on a metallic matrix. Since a decade, PDMC coatings are being synthesized and characterized widely because of their outstanding mechanical, magnetic, optical and multi functional properties compared to those of bulk materials [2,3]. In electrodeposited composite coatings, the rate of particle entrapment depends on many factors related to the size, density, zeta potential, and conductivity of the reinforced particles beside the plating parameters such as current density, pH, temperature and time. Abdel et al. have discussed the influence of these parameters on the particle incorporation rate and hence the structure, morphology and the properties of the composite coatings [4–6]. Agitation of the bath also appears to be an important factor in determining the particle content in metal matrix [7]. Over the past decades, many efforts have been carried out to improve the properties of nickel deposits by codeposition of micron sized particles such as carbides, oxides, nitrides, sulfides and diamond and their corresponding structures and properties were investigated by many researchers [8–17].

Nanocrystalline metals with grain size of less than 100 nm are a new and novel class of advanced materials, currently receiving considerable attention by the material scientists. In order to further enhance their properties, it is only recently that conventional electrocodeposition method has been extended to nanosized particles to produce nanocomposite deposits with finer grains and more compact structure. Several investigations have reported that the incorporation of hard inert nanoparticles such as carbon nanotubes (CNTs), CeO_2, TiO_2, SiC, Al_2O_3, Si_3N_4, ZrO_2, and diamond into metal matrix modifies the electro crystallization process of metal matrixes and thus, influences their mechanical and tribological properties [18–20]. Among the available nanosized particles, Titanium Carbo Nitride (TiCN) nanoparticles are increasingly attracting considerable scientific and technological interest by virtue of their higher abrasion resistance, hardness, lower friction coefficient and chemical stability at elevated temperatures [21–22]. TiCN is a solid solution of Titanium Nitride (TiN) and Titanium Carbide (TiC) and would incorporate the advantages and characteristics of both. It is due to its higher hardness and the presence of carbon acting as a lubricant leading to reduced friction and wear [23]. Especially in tribological applications, where abrasion is the dominant wear mechanism, TiCN is superior to TiN coating when machining stainless steel, high nickel alloys, cast iron and non-ferrous materials. Excellent surface finishes and close tolerances are obtained, even on super alloys and other difficult to machine materials for which TiC or TiN based coatings cannot be used [24,25]. Limited literature only is available on preparation and

* Corresponding author. Tel.: +91 4565 227550; fax: +91 4565 227773.
E-mail address: rameshbapugnk@cecri.res.in (G.N.K. Ramesh Bapu).

0257-8972/$ – see front matter © 2011 Elsevier B.V. All rights reserved.
doi:10.1016/j.surfcoat.2011.09.078

characterization of TiCN based electro composite deposits. Hellman et al. [26] have studied the effect of various hard coated steel coupons on thermo-oxidative stability in perfluoropolyalkyl ether lubricant and concluded that physical vapor deposited TiCN and electroless Ni–TiCN coatings have demonstrated superior corrosion resistance compared with uncoated steel. Lavrenko et al. [27] and Kumar et al. [28] have studied the polarization behavior of Ni–TiCN cermets in 0.2 mol^{-1} sulphuric acids and reported that factors like crevice corrosion due to the presence of pores and galvanic corrosion due to ceramic and binder phases determine the electrochemical properties of cermets. The primary target of the present study is to understand the effects of electrochemical parameters on the development of Ni–TiCN nanocomposite coatings codeposited using a Watts type nickel bath. The secondary aim of the present work is to characterize the composite deposits for hardness, wear resistance, and corrosion resistance and to examine the surface morphology and crystal structure.

2. Experimental

2.1. Effect of electrochemical parameters on electro codeposition of Ni–TiCN nanocomposite deposit

The electro codeposition was carried out in a 400 ml thermostatic glass cell where a steel plate (7.5×2.5×0.1 cm) and an electrolytic grade Nickel (Ni) sheet (7.5×2.5×0.5 cm) were used as the cathode and anode respectively. Both electrodes were kept vertically, facing each other as in conventional deposition. Prior to deposition, the substrates were mechanically polished to 0.08–0.12 μm surface roughness, degreased with acetone, cathodically cleaned and activated in a 10% sulphuric acid solution at room temperature. Ni and Ni–TiCN composite coatings were obtained on steel substrates from a Watts bath in which TiCN nanoparticles were suspended. The basic electrolyte compositions and experimental process parameter ranges used for the preparation of Ni–TiCN nanocomposite coatings are shown in Table 1. Weighed quantity of the TiCN nanopowder (Sigma Aldrich, USA), sized between 150 nm and 250 nm were thoroughly washed in acetone and dried. Then it was blended with 50 ml of the Watts nickel electrolyte taken in a mortar and the slurry was transferred to the main electrolyte. By means of a mechanically controlled stirrer, the particles were thoroughly stirred in the bath for 8 h and a mono dispersion was made in order to avoid agglomeration and sedimentation of the particles. Throughout the deposition time, the stirring was maintained so as to reach the particles towards the cathode surface and improve the incorporation rate. The extent of TiCN incorporation into nickel matrix was studied with respect to particle concentration ranged between 2 and 15 g l^{-1}, current density ranging from 2 to 10 Ad m^{-2}, bath pH from 2 to 5 and a bath temperature range of 30–70 °C. The amount of TiCN codeposited with nickel was analyzed gravimetrically by the anodic dissolution of a known weight of Ni–TiCN composite deposit (W_1 g) in a Watts bath, collecting TiCN particles in a weighed gooch crucible (G4) in which the composite deposit was suspended. TiCN was then thoroughly washed till free of Ni^{2+}, Cl^-, SO_4^{2-} and boric acid. Then, it was dried to a constant weight and the amount of TiCN in the composite (W_2 g) was thus obtained. The Ni contents of the composites (W_1–W_2 g) could be deduced from the differences between the weight of the composite and the TiCN there in. Using the mass of Ni and TiCN particles in the composite deposits and the density of Ni (8.9 g cm^{-3}) and TiCN particles (5.08 g cm^{-3}), the volume percent (vol.%) of TiCN incorporated in the Ni matrix was obtained within an accuracy of ±0.1%. Triplicate analyses were made in each case and the average values reported.

Table 1
Watts nickel electrolyte composition and the plating process parameters.

Electrolyte composition		Plating parameter ranges	
$NiSO_4 \cdot 6H_2O$	250 g l^{-1}	TiCN particle	2 to 15 g l^{-1}
$NiCl_2 \cdot 6H_2O$	45 g l^{-1}	Current density	2 to 10 Ad m^{-2}
H_3BO_3	30 g l^{-1}	pH	2 to 5
Sodium lauryl sulfate	0.1 g l^{-1}	Temperature	30 to 70 °C
		Stirring speed	600 r min^{-1}

2.2. Characterization of Ni–TiCN nanocomposite deposit

About 50 μm thick Ni and Ni–TiCN composite coatings were used for surface characterization, hardness and wear resistance studies. The crystal structure and orientation of the as-deposited Ni and Ni–TiCN nanocomposite coatings were examined by Philips X-ray diffractometer (XRD) using Cu Kα radiation and the grain size was determined from the diffraction data using Scherrer equation [29],

$$\text{Grain size (nm)} = \frac{0.9\ \lambda}{\beta \cos\theta} \quad (1)$$

where λ = 1.5406 A is the wave length of the radiation used, β is the Full Width Half Maximum (FWHM) and θ is the diffraction angle. The surface morphology was observed with a Hitachi 3000H scanning electron microscope (SEM).

The Vickers hardness measurements were done on the as-plated surface with MH6 Everone micro hardness tester applying a load of 50 gf for 15 s, using an indentation method [30]. To avoid the anvil effect, 50 μm thick deposit was used for measurements and the reported value was an average of six tests carried out on different locations on the samples.

The wear resistance performance was determined at 1 kg load at room temperature by a Taber rotary platform abrasion tester (Model 5135, USA) on sheet specimens (100×100×1 mm) using CS-10 Calibrase wheel [31]. Prior to wear test, all the contact surfaces were polished, cleaned in acetone and dried so that the tests were carried out under nominally dry sliding conditions. The test sample was mounted on rotary disk fixture and the wear resistance was characterized by weight loss. It was obtained by weighing the specimen before and after each experiment of wear test. The Taber wear Index (TWI) which is the weight loss in milligrams per 1000 cycles of abrasion was reported. Each test was repeated three times and the average was adopted as the experimental data.

Corrosion behavior of Ni and Ni–TiCN nanocomposite deposits was studied on 10 μm thick coatings by potentiodynamic polarization and electrochemical impedance spectroscopy (EIS), employing a three-electrode open cell with 1 cm^2 deposits as working electrode (WE), a platinum foil as counter electrode (CE) and saturated calomel electrode (SCE) as reference electrode (RE) using 3.5 wt.% NaCl solution at room temperature. Potentiodynamic polarization test was carried out by sweeping the potential at a scan rate of 1 mV s^{-1} in the range of ±200 mV with respect to open circuit potential (OCP). The corrosion potential (E_{corr}) and corrosion current density (I_{corr}) for the deposits were determined from the intersection of the cathodic and anodic Tafel curves by the Tafel extrapolation method [32–33]. The EIS tests were carried out using a Solartron Model SI 1255 HF Frequency Response Analyzer (FRA) coupled to a Princeton Applied Research (PAR) Model 273A potentiostat/galvanostat. The EIS measurements were obtained at OCP in frequency range from 100 kHz to 100 mHz with applied AC amplitude of 10 mV using EIS software model 398. All the recorded impedance spectra were analyzed as Nyquist diagrams.

3. Results and discussions

3.1. Effect of TiCN particle concentration in the bath and current density on vol.% TiCN incorporation in the composite deposit

Fig. 1 shows the relationship between the vol.% incorporation of TiCN in the composite deposit and the concentration of TiCN in the

plating bath at pH 4 and 50 °C over a current density range of 2 to 10 Ad m^{-2}. Irrespective of the applied current density, the particle incorporation increases sharply and reaches a maximum incorporation value with the increase of TiCN concentration in the plating bath up to 6 g l^{-1}. However, the TiCN content in the composite deposit decreased with further additions in the bath. Above 6 g l^{-1} TiCN additions, the stirring being insufficient to maintain all the particles in suspension, that lead to the agglomeration of the particles in the bath [34]. This accounts for the observed decrease in TiCN incorporation above 6 g l^{-1}.

Over the range of TiCN concentration in the bath, as seen in Fig. 1, the particle incorporation increased steadily up to 4 Ad m^{-2}, reached a maximum value and then the extent of codeposition got decreased. Beyond this limit, the hydrogen evolution reaction enhances thereby decreasing the current efficiency and codeposition of particles. As maximum codeposition and current efficiency is observed at 4 Ad m^{-2}, the diffusion-limited current for Ni deposition is 4 Ad m^{-2}. Beyond the limiting current density, as the reduction of nickel ions is controlled by concentration over potential, the current efficiency values and the amount of codeposited TiCN particles gradually decreased. This trend is found in good agreement with the codeposition of nano TiC particles in Ni matrix [35] and SiC particles in Ni–W–P [36]. According to the adsorption model describing the codeposition process, the codeposition of particles with the metal matrix depends on particle impingement and residence time at which it sits on the cathode surface. Once the particles are adsorbed on the cathode surface, they will be imbedded into the composite coatings [37]. The electrochemical mechanism depends on the field intensity between the interface of electrodes and solution and electric charges of the particle surface [38]. Under the influence of the applied electric field, the "ionic clouds" that is the particles surrounded by positively charged metal ions are transmitted to the cathode surface where adsorption and reduction of metal ions occurs. The particles will stay on the cathode surface by the external field and be captured by deposited metal. This explains the observed increase in incorporation with increasing current density up to 4 Ad m^{-2}.

3.2. Effect of pH and temperature on vol.% TiCN content of composite deposit

The influence of pH on TiCN incorporation is shown in Fig. 2. A smooth, uniform and semi-bright deposit containing 23.9 vol.% TiCN was obtained at 4 Ad m^{-2}, pH 4, and 50 °C for 6 g l^{-1} TiCN concentration in the bath. Depending on the bath pH, H cations or OH anions will get adsorbed on the surface of the particles and charge the surface. As maximum incorporation of TiCN was found at pH 4, TiCN particles under such conditions should have positive surface charge at pH<4 and negative surface charge at pH>4. The positively charged particles get attracted towards the cathode surface and entrapped between the nickel lattices. Increasing the pH beyond 4, the vol.% TiCN incorporation lowered drastically. As precipitation of Ni $(OH)_2$ occurs at pH above 5.0, a brittle deposit was obtained. As Nwoko and Shreir reported [39], the observed decrease in TiCN incorporation beyond pH 4 may be due to a decrease in the current efficiency of nickel deposition and an increase in the viscosity of the solution. The decrease in current efficiency lowered the rate of nickel deposition, with a consequent decrease in the incorporation of TiCN.

In Fig. 3 is shown the effect of operating temperature on the vol.% incorporation of TiCN for 6 g l^{-1} particle concentration in the bath at pH 4 and 4 Ad m^{-2}. As is seen, the incorporation of TiCN increased from 12.7 to 23.9 vol.% when the temperature was increased from 30 °C to 50 °C. Above this range, a decreasing trend was observed that may be due to the decrease in the current efficiency of nickel deposition at higher temperature.

3.3. SEM and XRD analyses of Ni and Ni–TiCN nanocomposite deposits

Fig. 4 depicts a typical scanning electron surface micrograph of the pure nickel, Ni-14.3 vol.% TiCN and Ni-23.9 vol.% TiCN nanocomposites processed in the Watts nickel solution containing (a) without TiCN (b) with 2 g l^{-1} TiCN and (c) 6 g l^{-1} TiCN in the bath respectively at pH 4, 50 °C and 4 Ad m^{-2}. Comparing the micrographs, an obvious difference can be found between the deposits with and without TiCN nanoparticles. The nickel deposits exhibit a poly crystalline structure (Fig. 4a) while the composite deposits show up a smooth, fine grained and compact structure without any dendrites. As illustrated, due to the nano size of TiCN particles, it is difficult to distinguish them from the nickel matrix in any of the composite coatings. An electrodeposited layer is a competitive step between crystal nucleation and growth. During codeposition of TiCN nanoparticles, the higher nucleation perturbs the growth of nickel matrix and results in a smaller grain size. The extent of codeposition is found to improve with increasing the concentration of TiCN particles in the Watts bath as seen in Fig. 4b and c.

The X-ray diffraction pattern of pure Ni and corresponding Ni-23.9 vol.% TiCN composite deposit is shown in Fig. 5 and the

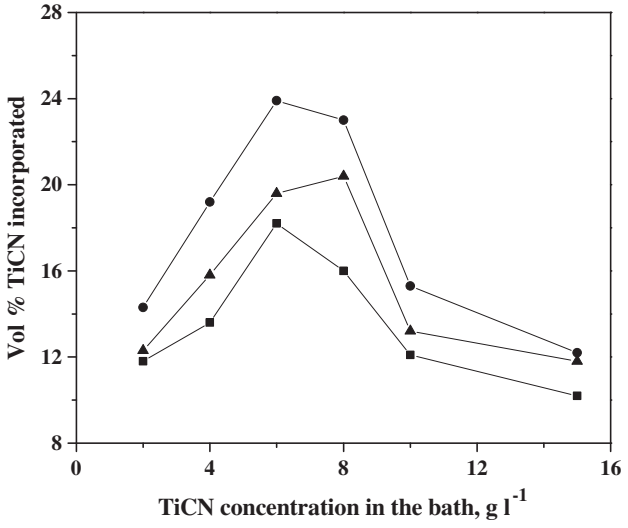

Fig. 1. Effect of TiCN concentration in the bath and current density on vol.% incorporation of TiCN in the Ni–TiCN composite deposit at pH 4 and 50 °C. ■–■–■– 2 Ad m^{-2}, ●–●–●– 4 Ad m^{-2}, ▲–▲–▲– 10 Ad m^{-2}.

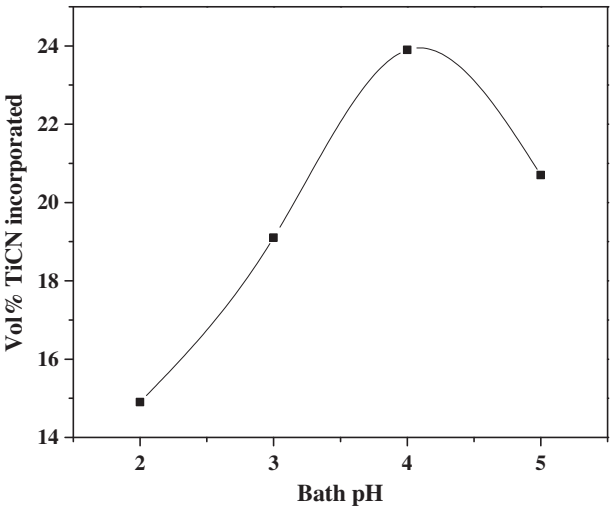

Fig. 2. Effect of bath pH on vol.% incorporation of TiCN in the Ni–TiCN composite deposit obtained at 6 g l^{-1} TiCN particle concentration at 4 Ad m^{-2} and 50 °C.

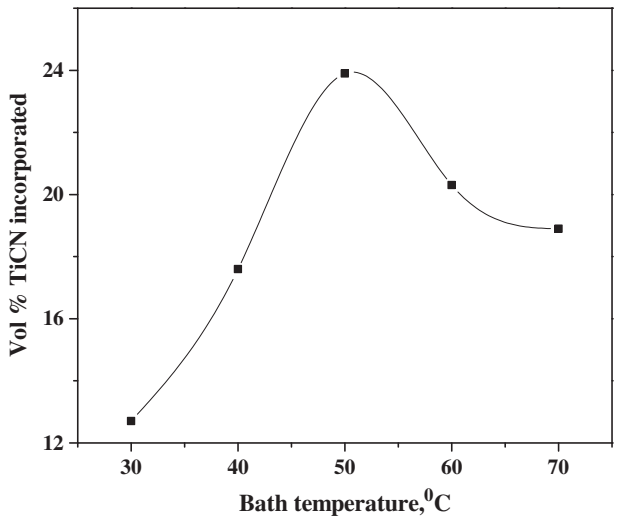

Fig. 3. Effect of bath temperature on vol.% incorporation of TiCN in the Ni–TiCN composite deposit obtained at 6 g l^{-1} TiCN particle concentration at pH 4 and 4 Ad m^{-2}.

calculated grain size and diffraction data in Table 2. The diffraction pattern of pure Ni (Fig. 5a) is characterized by a preferential orientation of (111) diffraction line, while those of Ni–TiCN composite deposit by (200) preferential orientation (Fig. 5b). It is of interest to note that the peak intensity of (200) line (Fig. 5b) is significantly increased than that of Fig. 5a due to the incorporation of TiCN particles. A small peak observed at $2\theta = 93.0774°$ may correspond to TiCN [40]. The observed shift of the (200) peak intensity is due to the incorporation of TiCN particles which significantly influences the crystal growth mode of Ni. The average grain size of Ni and Ni–TiCN is calculated to be 47 nm and 28 nm respectively. Lin and Huang [41] propose that codeposition of ceramic particles perturbs the crystal growth of Ni matrix by inducing an increase of the nucleation sites and consequently, a reduction in the crystallites size. Due to the incorporation of TiCN particles, the grain refinement resulted in a much smoother surface. This observation can be seen in the microscopic structure (Fig. 4b and c) of the composite deposit also.

3.4. Micro hardness of Ni and Ni–TiCN nanocomposite deposits

Table 3 shows the micro hardness of Nickel and Ni–TiCN nanocomposites obtained at 4 Ad m^{-2}, 50 °C, and pH 4 measured at a load of 50 g. The Vickers micro hardness of the Ni was measured to 220 VHN, while that of the Ni–TiCN nanocomposites containing 12.2, 14.3, and 19.2 vol.% TiCN were 450, 510, and 550 VHN, respectively. When the vol.% TiCN increased to 23.9, the micro hardness of the composite was 620 VHN. The improvement of the hardness of the composite coating is related to the change in grain size and structure of Ni crystallites and the hardening effect of the dispersoids in the composite. Nanoparticles scatter uniformly in the composite coating, so even the low fraction of ceramic phase is sufficient to significantly affect the mechanical properties of the nickel deposit. Moreover, under an applied load, the distributed nanoparticles would restrain the growth of the grains and the plastic deformation of the matrix by way of grain refining which would become stronger with increasing nanoparticles content in composite coatings. Similar trends had been reported with other ceramic particles in Nickel matrix [36,42].

3.5. Wear resistance of Ni and Ni–TiCN nanocomposite deposits

In Table 4 is shown the dependence of wear index, which is the weight loss in milligrams for 1000 abrasions on the vol.% of TiCN particles in the composite deposits. One can see that the incorporation of

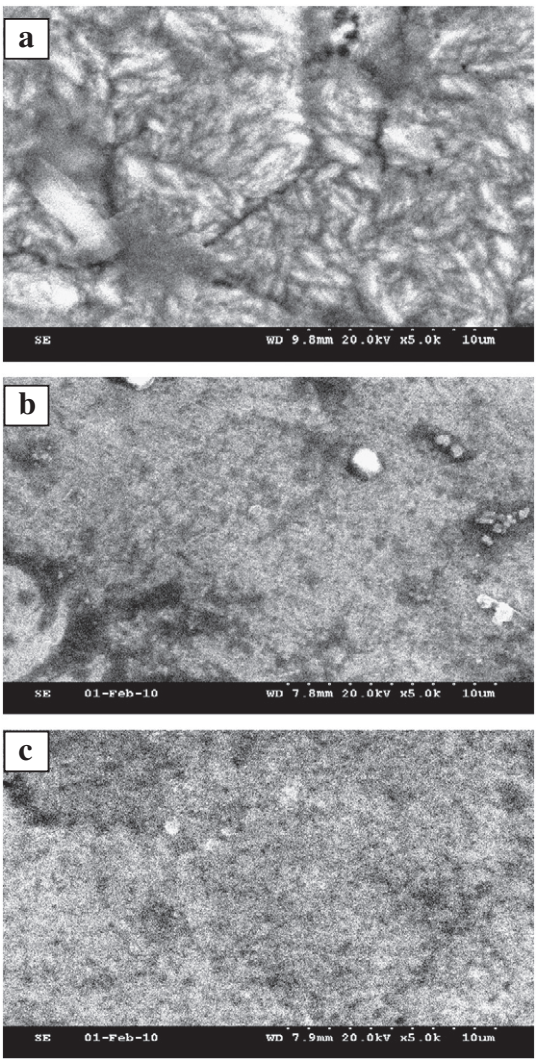

Fig. 4. SEM micrographs of the nickel, Ni-14.3 vol.% TiC and Ni-23.9 vol.% TiC nanocomposites obtained at current density 4 Ad m^{-2}, pH 4, and 50 °C from plating solution containing (a) 0 g l^{-1}TiCN, (b) 2 g l^{-1} TiCN, and (c) 6 g l^{-1} TiCN.

14.3, 19.2, and 23.9 vol.% TiCN in the composite deposit decreased the TWI about 32, 45 and 65%, respectively, in comparison to pure Ni deposit, which in turn indicate that the wear resistance of nickel deposit is obviously improved by incorporating TiCN particles. As Sun and Li discussed [43], this can be attributed to particle-strengthening effect by dispersing particles which inhabit the grain boundaries of the nickel deposits, and acts as obstacles to the grain movement and grain boundaries migration under cyclic normal load during Taber abrasion test. As is seen, Ni-23.9 vol.% TiCN nanocomposite shows the lowest TWI and the minimum wear loss.

Fig. 6 shows the worn surfaces of the composite coating and pure nickel coating. The fine striations along the sliding direction, probably from the sands plowing its way forward can be seen on the surface. The wear track of the nickel coating (Fig. 6a) shows signs of many grooves, pits, scuffing and plastic deformation whereas such pits and scuffing on the worn surface of the composite coating is significantly abated (Fig. 6b and c). The presence of grooves will cause larger wearing losses. The striations of the composite coating are found milder than that of the pure nickel coating, which is consistent with the wear data. So, the anti-wearing performance of pure nickel coatings is poorer than that of composite coatings. This is also expected based on the highest micro hardness (Table 3) shown by Ni-23.9 vol.% TiCN composite.

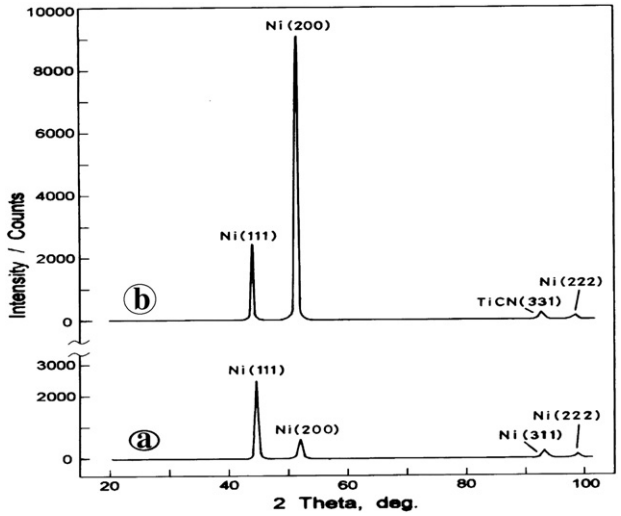

Fig. 5. XRD patterns of (a) pure Ni deposit and (b) Ni-23.9 vol.% TiCN composite obtained at current density 4 Ad m^{-2}, pH 4, and 50 °C from plating solution containing 6 g l^{-1} TiCN.

3.6. Corrosion resistance of Ni and Ni-TiCN nanocomposite deposits

Fig. 7 illustrates the potentiodynamic polarization curves for Ni and Ni–TiCN nanocomposite deposit obtained with different vol.% of TiCN particles in 3.5 wt.% NaCl solutions. The calculated corrosion current, corrosion potential and the Tafel slopes are summarized in Table 5. The data clearly reveals the enhancement of corrosion protection by TiCN reinforcement and the vol.% content of the dispersing particles. The embedded particles may act as inert physical barriers to the initiation and development of defect corrosion, modifying the micro structure of the nickel layer and hence improve the corrosion resistance [44].

From Fig. 7 and Table 5, it can be observed that in 3.5 wt.% NaCl solution the corrosion potentials of the Ni–TiCN nanocomposite deposits increased with increasing of the nano TiCN contents, while the corrosion current density of composite coating decreased. The lower corrosion rate of Ni–TiCN composite coating may be attributed on the one hand, to the nickel matrix and the higher contents of nano TiCN particles in the deposits, which intrinsically presents a higher corrosion resistance; on the other hand, to the reduction of the grain size and the structural modification of nickel crystallites expressed through the alteration of the preferred orientation with the incorporation of these particles (Table 2). As several researchers [45–47] pointed out, the dispersion of nanoparticle in the nickel layer results formation of many corrosion micro cells in which the nanoparticle act as cathode and nickel metal acts as anode because the standard potential of TiCN is more positive than nickel. Such corrosion micro cells facilitated the anode polarization. Therefore, in the presence of nanoparticles, localized corrosion is inhibited, and mainly homogeneous corrosion occurs [20]. Among these composites, the Ni-23.9 vol.% TiCN composite coating shows the highest corrosion resistance.

Table 2
X-ray diffraction data and grain size.

Figure	Deposit	Position (°2θ)	(hkl)	Height (cts)	Rel. int (%)	Grain size (nm)
Fig.4a	Nickel	44.4815	Ni (111)	2458	100	47
		51.8090	Ni (200)	626	26	33
		92.9578	Ni (311)	–	–	–
		98.3228	Ni (222)	–	–	–
Fig.4b	Ni–TiCN composite	44.4572	Ni (111)	2252	26	29
		51.8121	Ni (200)	8643	100	28
		93.0774	TiCN (331)	–	–	–
		98.4856	Ni (222)	–	–	–

Table 3
Micro hardness of Ni and Ni–TiCN composite deposit.

Deposit	Micro hardness ±20, VHN_{50}
Nickel	220
Ni-12.2 vol.% TiCN	450
Ni-14.3 vol.% TiCN	510
Ni-19.2 vol.% TiCN	550
Ni-23.9 vol.% TiCN	620

Table 4
Taber Wear Index of Ni and Ni–TiCN composite deposit.

Deposit	R_a, μm	Taber Wear Index (TWI[a])			Average TWI
		Cycle 1	Cycle 2	Cycle 3	
Nickel	0.43	38.2	30.1	28.6	32.3
Ni-14.3 vol.% TiCN	0.48	26.8	20.8	18.1	21.9
Ni-19.2 vol.% TiCN	0.51	21.2	17.8	14.4	17.8
Ni-23.9 vol.% TiCN	0.52	15.7	10.0	8.2	11.3

[a] Load 1 kg, CS 10 Calibrase wheel.

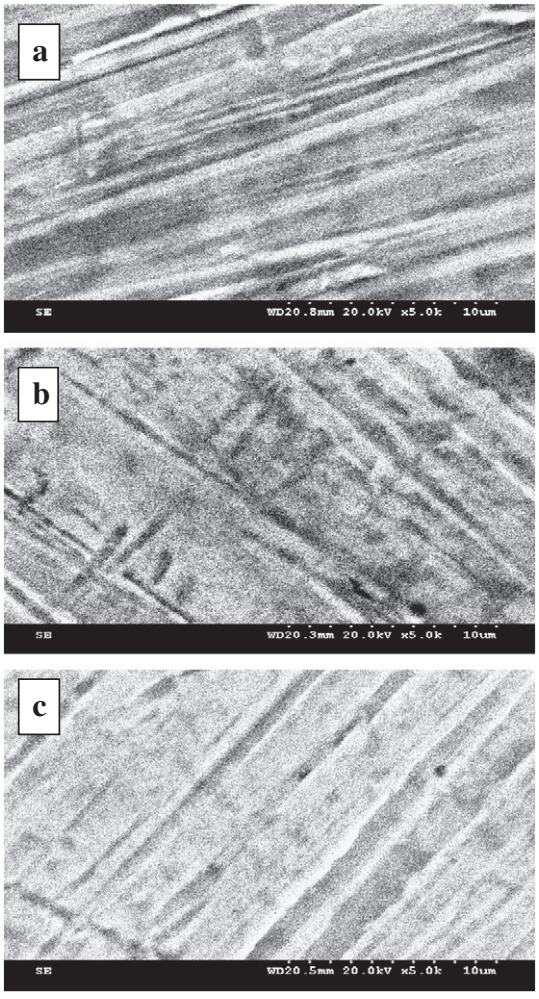

Fig. 6. SEM morphology of the wear track of nickel, Ni-14.3 vol.% TiCN and Ni-23.9 vol.% TiCN nanocomposites obtained at current density 4 Ad m^{-2}, pH 4, and 50 °C from plating solution containing (a) 0 g l^{-1}TiCN, (b) 2 g l^{-1} TiCN, and (c) 6 g l^{-1} TiCN.

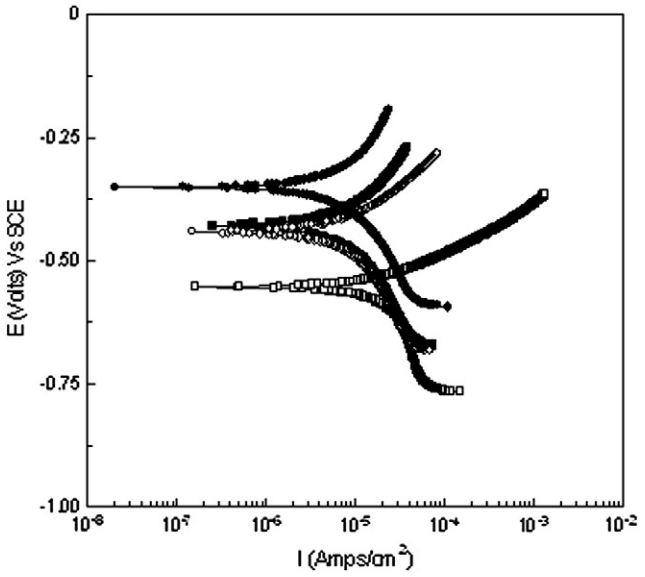

Fig. 7. Potentiodynamic polarization curves of Ni and Ni–TiCN composite deposit in 3.5 wt.% NaCl solutions obtained at current density 4 A d m^{-2}, pH 4, and 50 °C. □–□–□– Ni; ○–○–○– Ni-12.2 vol.% TiCN; ■–■–■– Ni-19.2 vol.% TiCN; ●–●–●– Ni-23.9 vol.% TiCN.

Fig. 8 shows the corrosion behavior of the Ni and Ni–TiCN nanocomposite deposits in 3.5 wt.% NaCl solution at their respective open circuit potentials using electrochemical impedance method and the calculated corrosion data is summarized in Table 5. All the curves appeared to be similar, consisting of a single semi-circle in the high frequency region signifying the charge controlled reaction. Moreover, the occurrence of a single semi-circle in the Nyquist plots indicates that deposit–solution interfaces exhibit charge transfer behavior and the corrosion process of these coatings involves a single time constant ($\tau = R_{ct} C_{dl}$) indicating existence of a double layer at deposit/electrolyte interface. This conclusion is found in good agreement with other reports available in the literature [48–50]. The high values of charge transfer resistance (R_{ct}), about 2 to 4 times more for the presently investigated Ni–TiCN composite deposit than Ni deposit, imply a better corrosion protective ability of the composite deposits. The capacitance value obtained for the composite deposit is found lower by about 75% in comparison to Ni deposit. In general, the C_{dl} value is related to the porosity of the coating. The low C_{dl} value confirmed that the Ni–TiCN composite deposit of present study was relatively less porous. By comparing the corrosion resistance of Ni and Ni–TiCN composite deposits, the latter deposit appeared to offer better corrosion protection. This seems to be logical, because even though the apparent area remains the same, the effective metallic area prone to corrosion is decreased considerably in the case of composite deposit. This would explain the reduced capacitance and increased polarization resistance data shown in Table 5.

Table 5
Corrosion behavior of Ni and Ni–TiCN composite in 3.5 wt.% NaCl solution.

Deposit	βa (mV decade^{-1})	βc (mV decade^{-1})	I_{corr}, μA cm^{-2}	$-E_{corr}$, V Vs SCE	R_{ct}, Ω cm^2	C_{dl}, μF cm^{-2}
Nickel	107	584	29.4	0.5539	1467	106.4
Ni-12.2 vol.% TiCN	332	339	12.5	0.4416	3921	35.6
Ni-19.2 vol.% TiCN	192	270	9.2	0.4299	6200	34.3
Ni-23.9 vol.% TiCN	111	209	6.6	0.3517	6950	25.2

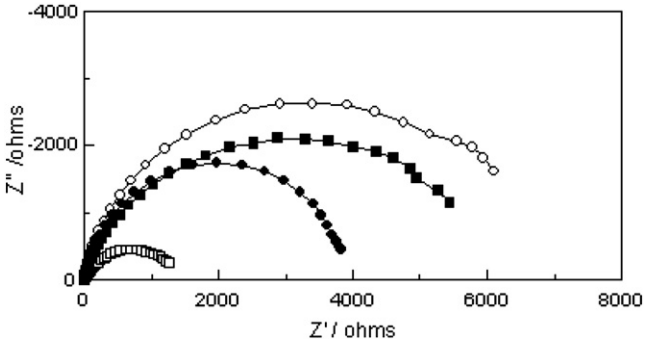

Fig. 8. Nyquist plots of Ni and Ni–TiCN composite deposit in 3.5 wt.% NaCl solutions obtained at current density 4 A d m^{-2}, pH 4, and 50 °C. □–□–□– Ni; ●–●–●– Ni-12.2 vol.% TiCN; ■–■–■– Ni-19.2 vol.% TiCN; ○–○–○– Ni-23.9 vol.% TiCN.

4. Conclusions

The properties of Ni–TiCN composite deposits was shown to depend on the grain size and the vol.% incorporation of TiCN particles as well as the structural modifications induced by the codeposition of particles. The average grain size of Ni and Ni–TiCN is calculated to be 47 nm and 28 nm respectively. In the present study, incorporation of TiCN particles had modified the surface morphology of Ni matrix by refining the grain size and exhibited a preferential (200) intense diffraction line. About 23.9 vol.% incorporation of TiCN in the nickel matrix was found at a current density of 4 A d m^{-2}, at pH 4, temperature 50 °C and, 6 g l^{-1} TiCN in the bath. Hardness, and wear resistance of the nanocomposite deposit was found to improve with increasing vol.% TiCN in the composite deposit. The grain size and the incorporation of TiCN nanoparticles were established to be the main factors for determining the best corrosion performance of Ni–TiCN composite deposits compared with electrodeposited nickel. In conclusion, the overall experimental findings illustrate that the incorporation of TiCN particles in Ni matrix influences drastically the crystal structure, orientation, hardness, wear resistance and corrosion resistance properties of nickel deposits.

Acknowledgments

The authors gratefully acknowledge the Department of Science and Technology of New Delhi, India (Grant No. SR/S3/ME/0012/2008) for financial support of this project under SERC scheme.

References

[1] M. Musiani, Electrochim. Acta 45 (20) (2000) 3397.
[2] C.T.J. Low, R.G.A. Wills, F.C. Walsh, Surf. Coat. Technol. 201 (1–2) (2006) 371.
[3] A.B. Viderine, E.J. Podlaha, J. Appl. Electrochem. 31 (2001) 461.
[4] A. Abdel Aal, K.M. Ibrahim, Z. Abdel Hamid, Wear 260 (2006) 1070.
[5] A. Abdel Aal, M. Barakat, R. Mohamed, 9th International Conference of Nano science and Technology, Basel, Switzerland, 2006.
[6] A. Abdel Aal, M. Baghat, M. Radwan, Surf. Coat. Technol. 201 (2006) 2910.
[7] R. Sen, S. Das, K. Das, Surf. Coat. Technol. 205 (2011) 3847.
[8] L. Chen, L.P. Wang, Z.X. Zeng, J.Y. Zhang, Mater. Sci. Eng., A-Struct. 434 (2006) 319.
[9] R. Sen, S. Bhattacharya, S. Das, K. Das, J. Alloys Compd. 489 (2) (2010) 650.
[10] V. Medeliene, Surf. Coat. Technol. 154 (2002) 104.
[11] S. Mohajeri, A. Dolati, S. Aezagholibeiki, Mater. Chem. Phys. 129 (3) (2011) 746.
[12] S.T. Aruna, V.K.W. Grips, K.S. Rajam, J. Alloys Compd. 468 (1–2) (2009) 546.
[13] L. Burzynska, E. Rudnik, J. Koza, L. Blaz, W. Szymanski, Surf. Coat. Technol. 202 (12) (2008) 2545.
[14] W.Y. Tu, B.S. Xu, S.Y. Dong, H.D. Wang, Mater. Lett. 60 (9–10) (2006) 1247.
[15] E. Pombei, L. Magagnin, N. Lecis, P.L. Cavallotti, Electrochim. Acta 54 (9) (2009) 2571.
[16] Q. Zhao, Y. Liu, H. Muller, G. Liu, Surf. Coat. Technol. 155 (2002) 279.
[17] P. Bercot, E. Pena, J. Pagetti, Surf. Coat. Technol. 157 (2002) 282.
[18] L. Wang, Y. Gao, Q. Xue, H. Liu, T. Xu, Mater. Sci. Eng. A 390 (2005) 313.

[19] C. Guo, Y. Zuo, J. Zhao, J. Xiong, Surf. Coat. Technol. 202 (2008) 3385.
[20] X.H. Chen, C.S. Chen, H.N. Xiao, Surf. Coat. Technol. 191 (2005) 94.
[21] S. Zhang, Mater. Sci. Eng 163 (1993) 141.
[22] M. Bhardwaj, R. Balasubramaniam, Mater. Charact. 59 (2008) 1474.
[23] E. Vancoille, J.P. Celis, J.R. Roos, Wear 165 (1993) 41.
[24] S. Zhang, Key Eng. Mater. 138 (40) (1998) 521.
[25] H. Zhang, S. Tang, J. Yan, X. Hu, Int. J. Refract. Met. Hard Mater. 25 (2007) 440.
[26] P.T. Hellman, J.S. Zabinski, L. Gschwender, C.E. Snyder Jr., A.L. Korenyi-Both, J. Synth. Lubr. 24 (1) (2007) 1.
[27] V.A. Lavrenko, A.D. Panasyuk, M.B. Desmaison, V.A. Shvets, J. Desmaison, J. Eur. Ceram. Soc. 25 (2005) 1813.
[28] B.V.M. Kumar, R. Balasubramaniam, B. Basu, J. Am. Ceram. Soc. 90 (2007) 205.
[29] S.T. Huang, The X-ray study for solid-state, Higher Education Publishing House, Beijing, 1985.
[30] ASTM B578-87, Standard test method for micro hardness of electroplated coatings, Philadelphia, vol 02.05, 1999.
[31] ASTM D4060-95, Standard Test Method for Abrasion Resistance of Organic Coatings by the Taber Abraser, Philadelphia, vol 06.01, 1999.
[32] C.M.A. Brett, A.M. Oliviera Brett, Oxford University Press, 1998, p. 114.
[33] E. Poorqasemi, O. Abootalebia, M. Perikaria, F. Haqdara, Corr. Sci. 51 (2009) 1043.
[34] G.N.K. Ramesh Bapu, M.M. Yusuf, Mater. Chem. Phys. 36 (1993) 134.
[35] H. Lee, H. Lee, J. Jeon, Surf. Coat. Technol. 201 (2007) 4711.
[36] A. Abdel Aal, El-Sheikh, Y.M.Z. Ahmed, Mater. Res. Bull. 44 (2009) 151.
[37] J. Fransaer, J.P. Celis, J.R. Roos, J. Electrochem. Soc. 139 (2) (1992) 413.
[38] R. Xu, J. Wang, L. He, Z. Guo, Surf. Coat. Technol. 202 (2008) 1574.
[39] V.O. Nwoko, L.L. Shreir, J. Appl. Electrochem. 3 (1973) 137.
[40] G. Shen, K. Tang, C. An, Q. Yang, C. Wang, Y. Qian, Mater. Res. Bull. 37 (6) (2002) 1207.
[41] C.S. Lin, K.C. Huang, J. Appl. Electrochem. 34 (2004) 1013.
[42] Y. Yao, S. Yao, I. Zhang, W. Wang, Mater. Lett. 61 (2007) 67.
[43] X.J. Sun, J.G. Li, Tribol. Lett. 28 (2007) 223.
[44] E.A. Pavlatou, M. Stroumbouli, P. Gyftou, N. Spyrellis, J. Appl. Electrochem. 36 (2006) 385.
[45] L. Shi, C. Sun, P. Gao, F. Zhou, W. Liu, Appl. Surf. Sci. 252 (2006) 3591.
[46] L.Y. Wang, J.P. Tu, W.X. Chen, Y.C. Wang, X.K. Liu, C. Olk, D.H. Cheng, X.B. Zhang, Wear 254 (2003) 1289.
[47] K.H.W. Seah, M. Krishna, V.T. Vijayalakshmi, J. Uchil, Corros. Sci. 44 (2002) 917.
[48] T. Rabizadeh, S.R. Allahkaram, Mater. Des. 32 (2011) 133.
[49] J.N. Balaraju, V. Ezhilselvi, V.K. William Gripps, K.S. Rajam, Electrochim. Acta 52 (2006) 1064.
[50] T.S.N. Sankaranarayanan, I. Baskaran, K. Krishnaveni, S. Parthiban, Surf. Coat. Technol. 200 (2006) 3438.